Implications of inorganic contaminant leaching for point-of-use water treatment technologies providing "safe" drinking water: Arsenic leaching from ceramic water filters

Michael V. Schaefer, John D. Montgomery Postdoctoral Fellow, 2019-2020 and Ninh Le, Soka University of America Class of 2022

Summary

This paper briefly reviews the production and use of ceramic water filters (CWF) as an appropriate technology for point-of-use (POU) household water treatment. The efficacy of CWFs is traditionally quantified through removal efficiency (i.e. log-reduction) of pathogenic or indicator bacteria. However, depending on specific production factors (source clay material, kiln firing temperature, input water source) CWFs may also produce water contaminated with arsenic, fluoride, or other inorganic contaminants. The policy questions that arise concern how to properly regulate and manage total water quality in a household POU water treatment context inclusive of both pathogens and inorganic contaminants. This policy brief reviews the often-overlooked inorganic contaminant water quality issue by focusing on the mechanism that leads to arsenic leaching from CWFs. Estimates of total arsenic burden are provided, and recommendations for assessing and mitigating arsenic leaching from existing CWF manufacturing facilities are developed. Finally, the policy brief provides recommendations for how to predict arsenic leaching prior to siting and construction of new CWF manufacturing facilities and advocates that inorganic contaminant leaching should be included in assessing the overall efficacy of CWFs in providing safe drinking water.

Abstract

The ceramic production process involves mineralogical changes to arsenic (As) and iron (Fe) induced by firing typically at temperatures of 800-900 °C. Ceramic firing at 800-900 °C causes mineralogical changes to arsenic (As) and iron (Fe) that increase As leaching from CWF material compared to source clay. We present wet chemical extraction data combined with X-ray diffraction and X-ray absorption spectroscopy to show that firing converts As primarily associated with Fe-oxides to ~30% As in a phase similar to arsenate evaporite minerals. The higher solubility of evaporite As phases combined with increased As-Fe bond distance and Fe incorporation into the ceramic matrix are each consistent with the observed increase in As leaching. Improved understanding of molecular-scale processes governing increased As leaching from CWFs provides a basis for assessing arsenic leaching potential prior to CWF factory capital investment as well as engineered solutions (e.g. modified firing temperature, material amendments, enhanced leaching prior to distribution) to mitigate As exposure from CWFs.

Introduction

Point of use (POU) water filtration is an essential step in removing pathogens from drinking water in regions with poor source water quality or where water quantity limitations require storage under aseptic conditions[1]. An effective POU option is the ceramic water filter (CWF), which can be produced using locally available clay, water, and burnout material (e.g. rice husk, saw dust)[2,3]. Unlike typical ceramic materials, CWFs are designed to be porous. This is achieved by controlling the ratio of burnout material, where more saw dust or rice husk creates additional pore spaces in the ceramic. Pathogens are removed from water when the pore size is small enough that water is able to pass through the pores but bacteria are not. However, pore size must be optimized so that flow rates are high enough to be practical useful while pores remain small enough to effectively filter out pathogens. Silver has antimicrobial properties and is often added to CWFs to provide an additional layer of safety. CWFs are typically integrated into a safe water storage container to avoid recontamination between filtration and consumption (Figure 1).

Figure 1. Conceptual representation of a ceramic water filter integrated into a safe storage container. Image courtesy of Potters for Peace (pottersforpeace.org).

Previous studies of CWF performance have indicated up to 4-log (99.99%) reduction in bacteria and 2-log (99%) reduction in viruses[4] which, combined with low production cost, widespread availability of source materials, and ease of operation, have made CWFs an attractive POU water treatment option globally (Figure 2). In Cambodia two known factories currently produce and distribute a combined 5000-6000 CWFs per month.

However, it is increasingly recognized that CWF materials have the potential to leach arsenic (As) especially during the initial stages of use[5–7] leading to a tradeoff in biologically and chemically safe water.

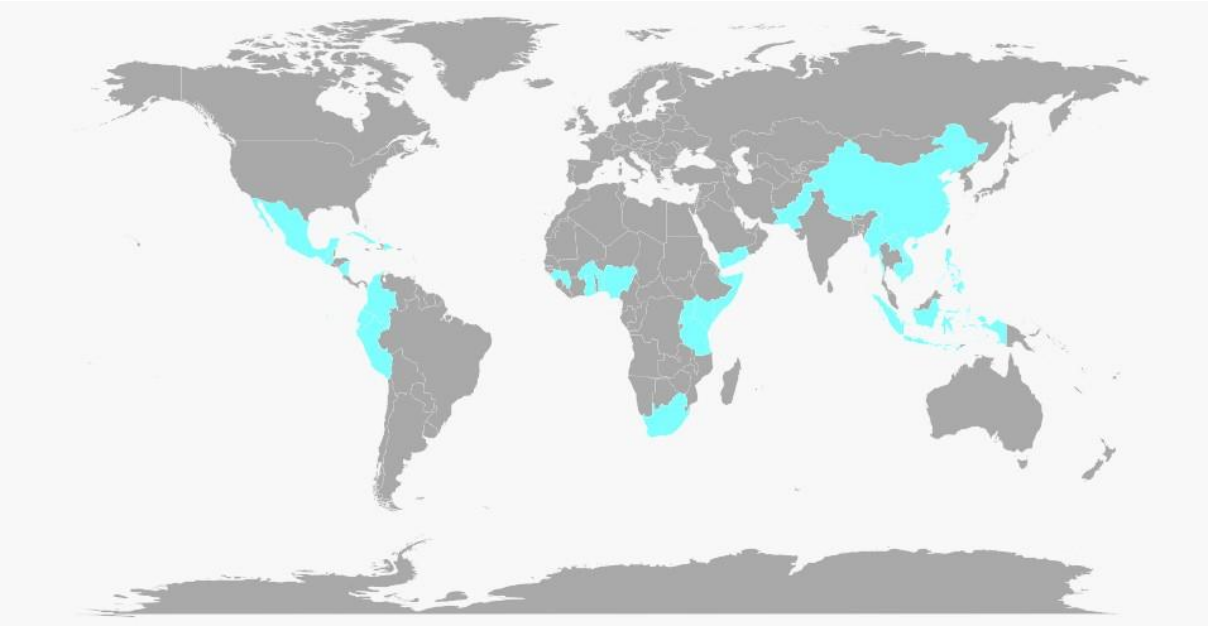

Figure 2. Highlighted countries have at least one ceramic water filter (CWF) production facility that is either currently operating or operated in the past. Data were compiled from peer-reviewed literature, the Potters for Peace CWF filter production facility database (https://pottersforpeace.org/?page_id=360), and personal communication with filter factories. This list is likely not exhaustive.

Arsenic is toxic and causes systemic adverse health effects when consumed above recommended health guidelines[8,9] including increased rate of cancers[10–13], cardiovascular disease[14], and susceptibility to infectious disease[15]. In addition, As exposure is correlated with increased incidence of type 2 diabetes[16]. The World Health Organization recommended limit for safe drinking water is 10 parts per billion (ppb), although some countries including Cambodia continue to use an older standard of 50 ppb for regulatory purposes. Despite official guideline values there is no safe level of As consumption. Because of the potent toxicity of As, it is imperative to understand the mechanisms leading to As leaching from CWFs so that human exposure to As can be minimized. Improved mechanistic understanding of As release provides a pathway for developing both screening protocols to avoid siting production facilities near source clays prone to significant As leaching as well as developing engineered solutions to mitigate As exposure from CWFs at existing facilities.

In this study we documented As leaching from CWFs and compared iron (Fe) and As solubilization and chemistry from unfired source clay and fired CWF material from a CWF production facility in Kandal Province, Cambodia. Using a combination of wet chemical extractions and X-ray techniques, we identified changes in Fe and As mineralogy and chemical binding before and after firing. Understanding of chemical mechanisms responsible for As leaching provides a framework for how to avoid clay sources with the potential to create As-producing ceramic and how to modify existing CWF production processes to reduce human exposure to As from CWFs.

Materials and Methods

Source clay and CWF sample collection

Samples of source clay and CWF were taken from the production facility at Resource Development International (RDI) in Kandal Province, Cambodia. The clay sample was collected prior to mixing with water and rice husk[2], and the CWF sample was collected immediately following firing, prior to flowrate testing. The entire CWF (~4.3 kg) was crushed and homogenized prior to further analyses.

Water and Acid Extraction

Water extractable As was determined from clay and CWF suspended in deionized water at a solids concentration of ~10 g/L. Suspensions were agitated on a shaker table operating at 120 rpm. Aqueous samples were removed and filtered (0.22 micron) after 1 hour (typical for water residence time in an operational filter) and 37 days prior to determination of aqueous As and Fe concentrations using inductively coupled plasma optical emission spectroscopy (ICP-OES). Water extractions were performed in triplicate. Hydrochloric acid (HCl) extractable As and Fe was determined by mixing 1 g of sample with 30 mL of 2 N HCl (trace metal grade). Suspensions were shaken for 23 hours on a shaker table at 120 rpm and then filtered (0.22 micron) prior to analysis using ICP-OES. HCl extractions were performed in triplicate.

Solid phase characterization

X-ray Fluorescence

Bulk elemental concentrations of solid samples were determined using a Spectro Xepos energy dispersive X-ray Fluorescence (ED-XRF) spectrometer with a 50 watt X-ray tube operating at 60 kV. Approximately five grams of each sample was ground with an agate mortar and pestle and placed in a plastic cup fitted with Prolene polypropylene film (Chemplex). Reported concentrations and errors result from analysis of five distinct locations on each sample.

X-ray diffraction

Samples were finely ground with an agate mortar and pestle and then mounted as a randomly oriented powder on an aluminum holder. Data were collected between 2-60° 2**θ** with a 0.01° step size and dwell time of 4 s using a Siemens D500 XRD with a Cu K**α** X-ray source operating at 40 kV. Alignment was calibrated using a quartz slide, and quartz in the samples was used as an internal calibration check. Background removal was performed using JADE software (MDI). Peak positions and intensities were assigned using reference diffraction data from the Joint Committee on Powder Diffraction Standards mineral database.

X-ray absorption spectroscopy data collection

X-ray absorption spectroscopy data were collected at the Stanford Synchrotron Radiation Lightsource (SSRL). Arsenic data were collected on Beamline 9-3 in a He cryostat environment at 15K, and fluorescence signal was measured using a 30-element Ge detector (Canberra). Energy selection was achieved using a Si(220) double monochromator and calibrated to the white line position of sodium arsenate set at 11875 eV. Samples were scanned from 11635 to 11835 eV in 5 eV steps, from 11835 to 11900 in 0.35 eV steps, and to k = 15 $Å^{-1}$ in 0.05 $Å^{-1}$ steps.

Iron K-edge data were collected on Beamline 4-1 in liquid N_2 cryostat (77K) and fluorescence signal was measured using a PIPS detector. Energy was selected using a Si(220) double monochromator and in-line calibration was achieved using an Fe foil and setting the inflection point to 7112 eV. Samples were scanned from 6800 to 7090 eV in 5 eV steps, from 7090 to 7142 eV in 0.25 eV steps, and to k = 13 $Å^{-1}$ in 0.05 $Å^{-1}$ steps.

XAS data analysis

Arsenic XAS analysis

The X-ray absorption near edge structure (XANES) portion of As K-edge data was analyzed using a linear combination fit (LCF) approach to determine dominant As oxidation state in each sample. Data reduction and analysis for LCF fitting were performed in Athena[17]. Replicate scans were merged and linear and cubic functions were fit to the pre- and post-edge regions of the spectrum, respectively. The edge jump was then normalized to one. Reference standards of arsenite [As(III)] and arsenate [As(V)] adsorbed on ferrihydrite were used as standards, and data were fit between 11,842-11,892 eV. The inclusion of additional standards did not improve LCF fits of the XANES region. Arsenic extended X-ray absorption fine structure (EXAFS) data were also

analyzed using LCF with As(V)- and As(III)-ferrihydrite, sodium arsenate, and arsenian pyrite as reference standards. Fits were performed on k^2-weighted data over the range of 3-12 $Å^{-1}$.

Multi-shell fitting of As EXAFS spectra was performed using FEFF 6 and IFEFFIT implemented in the Demeter software package.[17] The CWF spectrum was fit over a k range of 5-12.5 $Å^{-1}$ to minimize contributions from multiple scattering within the AsO_4 tetrahedron, while the source clay was fit over the k range of 4-12.5 $Å^{-1}$. The lower limit of this range was chosen to exclude contributions from As-O-O-As multiple scattering paths in the Fourier transform. The data was Fourier transformed using a Hanning window function. Least-squares, shell-by-shell fitting of the k^2-weighted spectra were then calculated over the R range of 1-4 Å. Theoretical phase-shift and amplitude parameters were then calculated using Artemis as an interface to the *ab initio* FEFF 6 code[18]. Scattering paths were generated using Na_2AsO_4 •$7H_2O$[19], nontronite[20], and Yurmarinite[21,22] as initial input structures. Scattering paths describing the As-O contributions from the As^V tetrahedron for both samples were obtained from Na_2AsO_4 •$7H_2O$. The Fe single scattering paths describing the second shell of the CWF spectrum and Fe and Si in the second shell of the source clay spectrum were constrained by assigning S_0^2=1, and the coordination number of each scattering species was also fixed. Parameters describing E_0, ΔR and σ^2 were allowed to vary with the fit.

Iron XAS analysis

The XANES region of Fe XAS spectra was analyzed qualitatively by comparing the pre-edge peak intensity of clay and ceramic samples at ~7114 eV.

Multi-shell fitting of the Fe EXAFS was performed similarly to the As EXAFS analysis. For the clay, 6-line ferrihydrite[23] was used as an initial input structure. The coordination number was fixed over the course of the fits, as were the $\boldsymbol{\sigma}^2$ values for scattering atoms in the 2nd shell. Fitting was performed in R-space from 1.2-3.7 Å, and in K-space from 3.5-12 $Å^{-1}$. For the CWF, magnetite[24] and hematite[25] were used as input structures to provide both octahedral and tetrahedral initial paths. Coordination numbers were fixed at the values generated by FEFF, and the amplitude-reduction factor for Fe scatterers in the 2nd shell was fixed at 0.8. All other parameters were allowed to vary freely.

Results and Discussion

Mineralogy and chemical composition

X-ray diffraction patterns of the source clay and CWF material show that firing induces changes in source clay mineralogy typical of vitrification and conversion to ceramic material (Figure 3).[26] Low-angle peaks (<20° 2**Θ**, large d-spacing) in the source clay are indicative of layer silicates including illite, kaolinite, and phyllosilicates. After firing at 866 °C low angle peaks are not present in the CWF material due to dehydroxylation of kaolinite at ~450 °C and illite decomposition which begins at 800-850 °C[26,27]. Peaks indicative of quartz are present in both samples, but the intensity of quartz peaks is higher in the source clay than in the CWF. **α**-quartz begins to transition to **β**-quartz at ~750 °C[26]. Some layer silicates such as muscovite have overlapping peak positions with quartz and the presence and transformation of these phases during firing may also lead to changes in peak intensity.

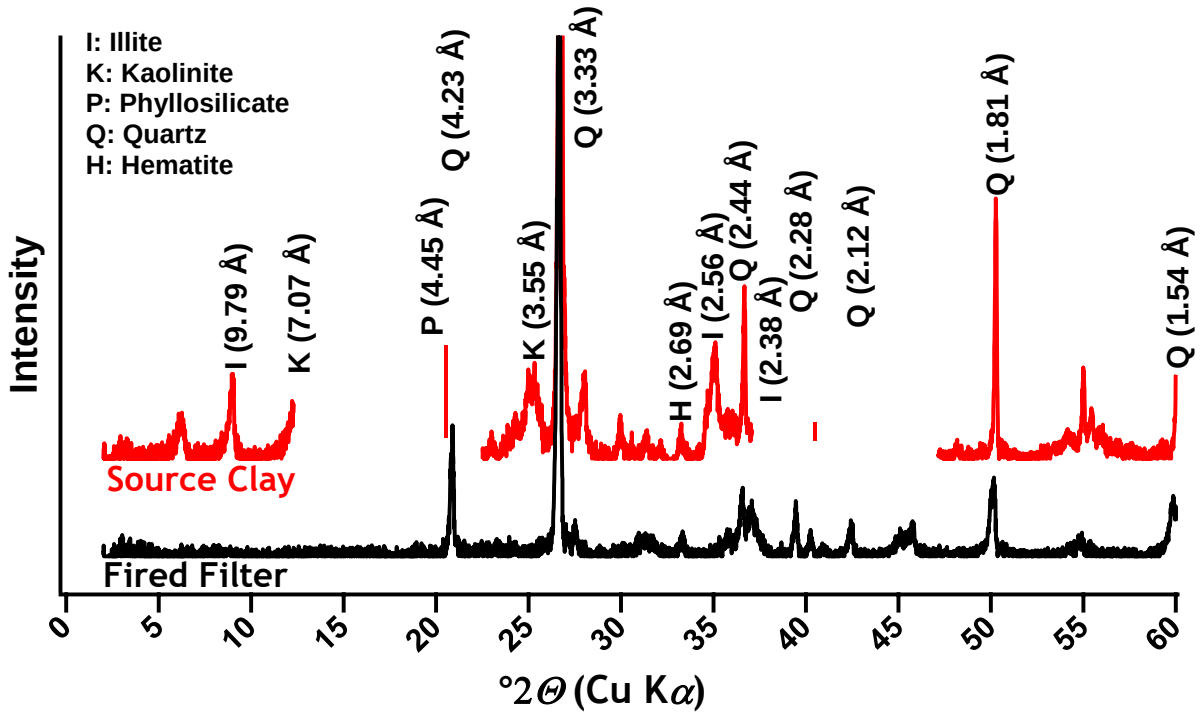

Figure 3. Powder X-ray diffraction patterns of source clay (red) and CWF (black). The y-axis is scaled so that the main quartz peak is cut off in each pattern for clarity. The normalized intensity of the quartz peaks is lower after firing, and low-angle peaks are present only in the source clay.

Elemental abundance was similar between source clay and CWF based on XRF measurements. Arsenic content was 14 and 16 ppm for clay and CWF, respectively, and Fe content was 4.4% and 5%. Loss of structural water during firing may have concentrated elements other than oxygen.

Water and HCl Extractions

Firing increases water soluble arsenic by a factor of 41 compared to the source clay, but no significant Fe is water soluble in either sample (Figure 4). Similarly, HCl-extractable As is 18 times higher in CWF than source clay but HCl-extractable Fe exhibits the opposite result, where HCl-extractable Fe from source clay is 8 times higher than from CWF (Figure 4). Both conversion of less stable Fe oxides in the source clay to more stable forms such as hematite and/or incorporation of Fe into the ceramic framework would decrease Fe solubility. Changes in As and Fe solubility indicate an apparent decoupling of As and Fe, whereby CWF firing increased As solubility and decreased Fe solubility. Arsenic therefore appears to transition from being primarily associated with Fe oxides in the source clay to a discrete phase following firing. To probe the chemical changes that result from firing we utilized Fe and As X-ray absorption spectroscopy.

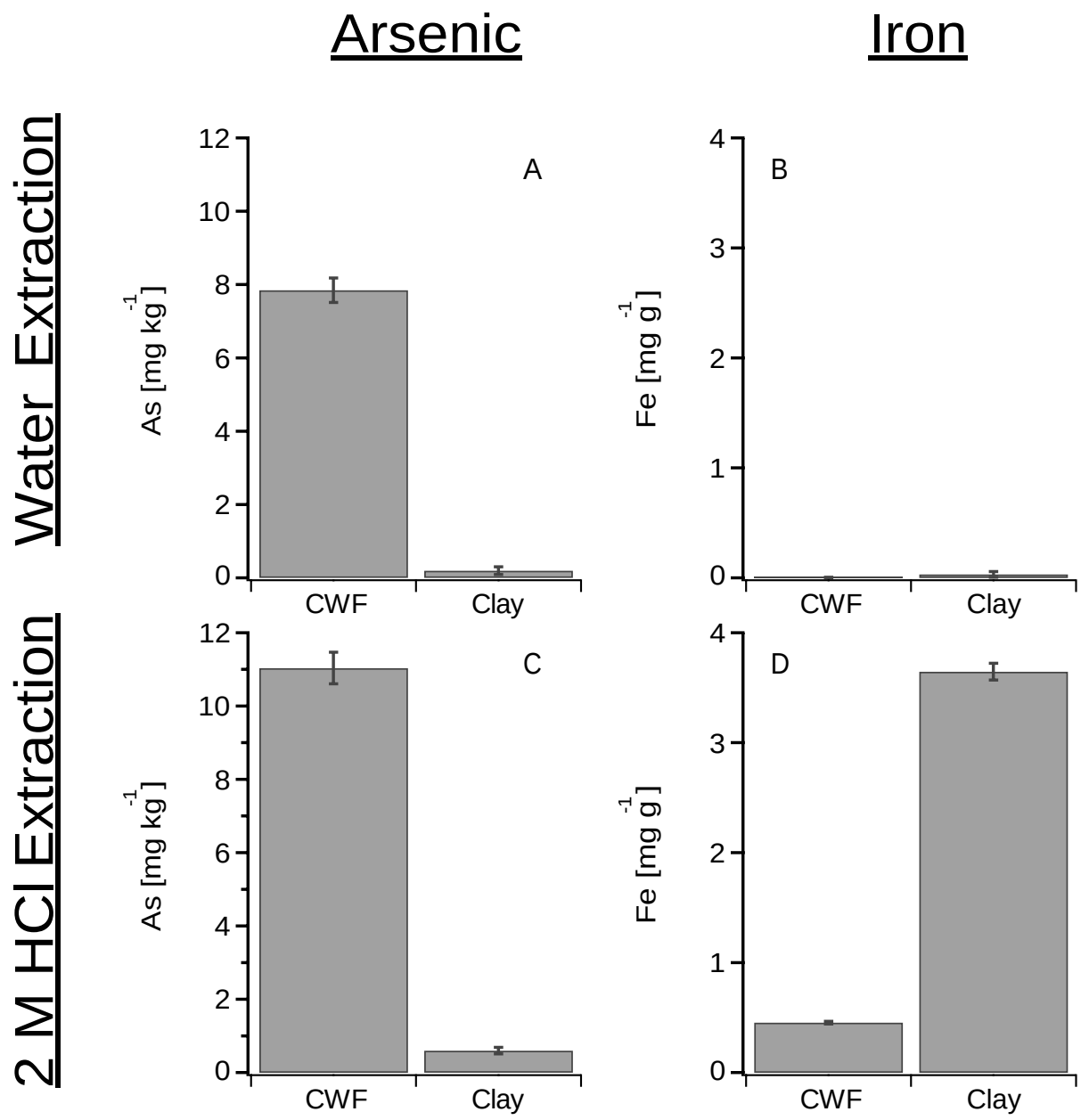

Figure 4. Water (A, B) and 2 M HCl (C, D) extractable arsenic (mg kg^{-1}) and iron (mg g^{-1}) for CWF and source clay. Water extractable arsenic (A) is 41 times higher in CWF than clay and water extractable iron (B) is near detection in both samples. HCl extractable arsenic (C) is 18 times greater in CWF while HCl extractable iron (D) is 8 times greater in source clay. Error bars represent standard error (n=3).

Mineral Transformation

Firing results in conversion of Fe in soils (Fe in clay minerals and oxides) to a phase consistent with observations of Fe(III) in Fe-rich glass and ceramic materials.[28] Conversion

of Fe (oxyhydr)oxides initially present in the source clay to Fe(III) consistent with a silicate matrix is also consistent with the decrease in HCl-soluble Fe after firing (Figure 4).

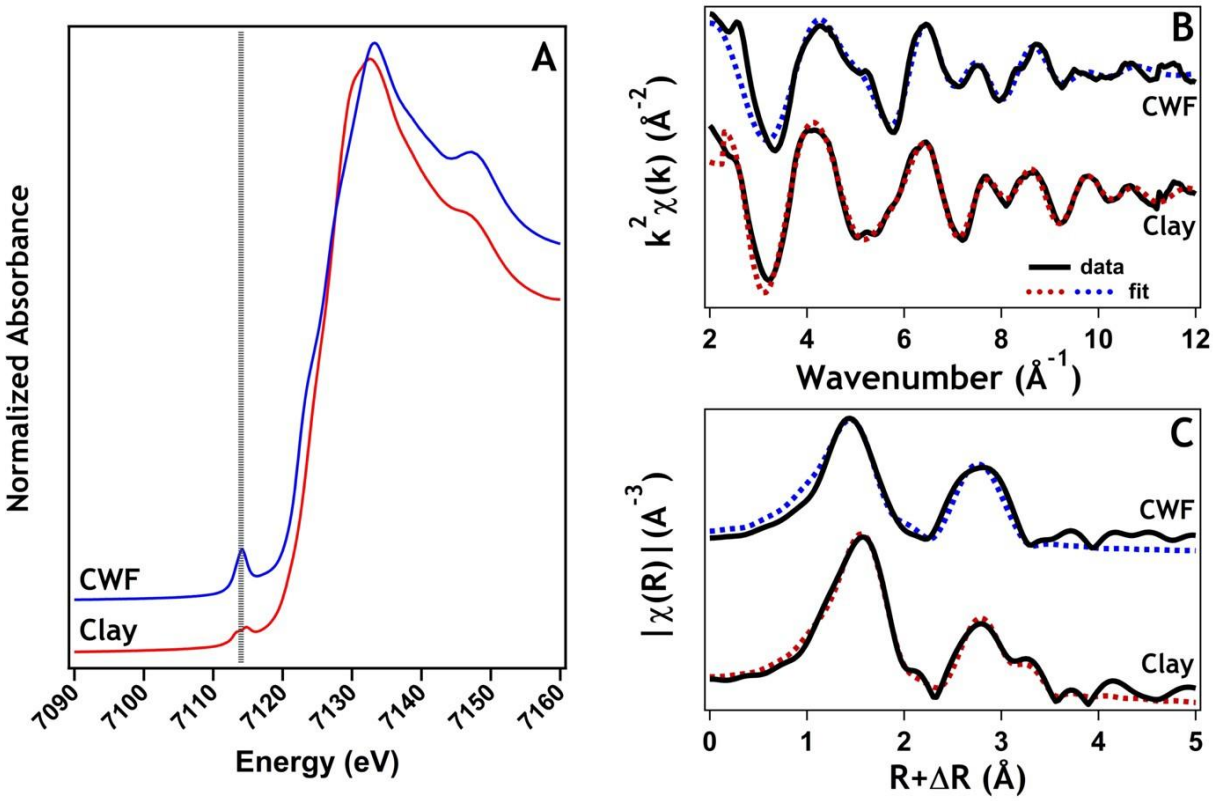

Figure 5. Iron K-edge X-ray absorption spectra. (A) XANES spectra of raw clay and fired ceramic materials. Gray vertical line indicates 7114 eV highlighting the pre-edge feature that forms following firing. Fe K-edge EXAFS data (solid black lines) and results of multi-shell fitting (dashed lines) of clay and CWF samples. (B) Fe EXAFS data weighted by k^2 and (C) Fourier transform uncorrected for phase shift.

Arsenic XANES spectra indicated that the raw clay contained 80% As(V) and 20% As(III) while CWF material contained 94% As(V) and 6% As(III). The value of As(III) for CWF is close to or within the detection limit using LCF XANES analysis, and therefore it is possible that As(V) is the only As species in CWF material.

Modeling of As EXAFS data showed that the contribution of As-Fe backscattering decreased following firing (Figure 6), consistent with a partial transition to an arsenate phase not associated with Fe-oxides. In addition, the As-Fe distance increased from 2.77 Å to 3.27 Å after firing. Formation of 28% As(V) represented by Na_2HAsO_4 may at least

partially explain the rapid initial leaching and high aqueous concentrations (>1,000 μg L^{-1}) observed during CWF flushing and initial use[7].

We propose that under the conditions in the kiln (>866 °C, near atmospheric pressure, oxygenated atmosphere) arsenate initially associated with Fe-oxides and clay minerals undergoes reactions similar to fumarolic arsenate formation. Fumarolic arsenates form under conditions of high temperature, low (near atmospheric) pressure, high oxygen fugacity, and gaseous transport of constituents[24], conditions similar to kiln firing of CWFs. Under these conditions fumarolic arsenates form below 1000 °C either through homogeneous gas-phase reactions or gas-rock interactions at temperatures >450 °C and most likely in the range of 500-750 °C[29].

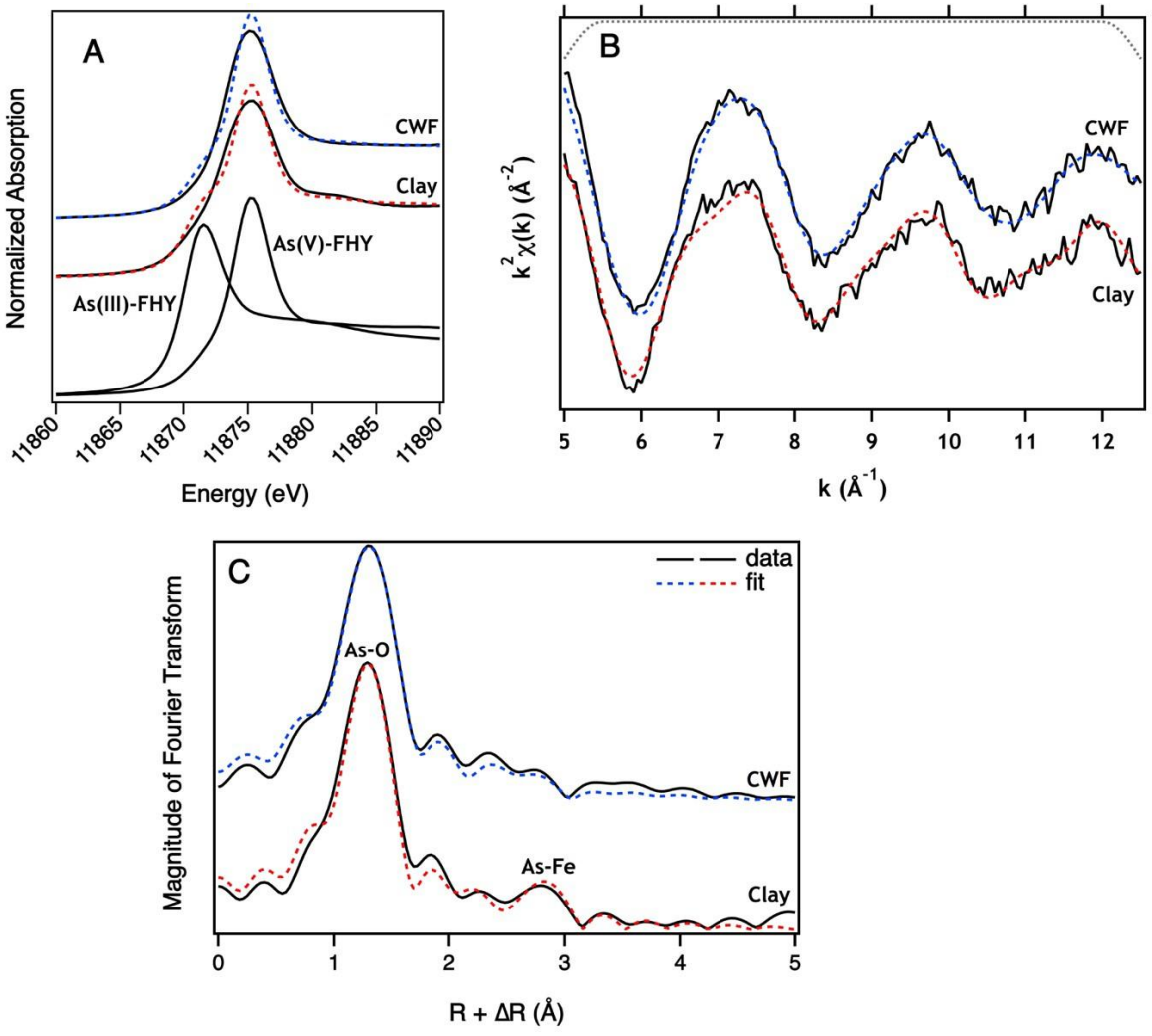

Figure 6. Arsenic K-edge XAS data of CWF and clay samples. (A) Linear combination fitting (LCF) analysis of the XANES region shows that As(V) is the dominant species in both samples. (B) Shell-by-shell fitting of the k^2-weighted EXAFS spectra and (C) Fourier

transform indicate the presence of Fe in the second shell in the clay sample, but this spectral feature disappears following firing. Distances in (C) are uncorrected for phase shift. In all plots, solid black lines indicate data and dashed color lines indicate model fits.

The As solid-phase concentration in both clay and CWF is too low to detect fumarolic arsenate minerals using X-ray diffraction, and we are currently unable to isolate or purify the As mineral phase for mineral-specific identification. However, shell-by-shell modeling of As EXAFS data in general supports As coordination similar to fumarolic arsenate minerals at least through the decrease in Fe backscattered intensity observed in As EXAFS spectra.

Implications for CWF Production and Use

Household use of CWFs combined with safe water storage remains an effective, low-cost technology for point-of-use pathogen removal from drinking water. However, during ceramic firing changes in Fe mineralogy from octahedrally-dominated Fe to tetrahedrally-dominated Fe limit available sorption sites for As in the CWF material. This important change in mineralogy in part increases the solubility of As in CWFs, leading to As contamination of otherwise-safe drinking water. Arsenic phase changes further increase overall As solubility in CWFs. Together these processes increase As leaching into product water during initial CWF use, resulting in As hazard associated with CWF production and use (Figure 7).

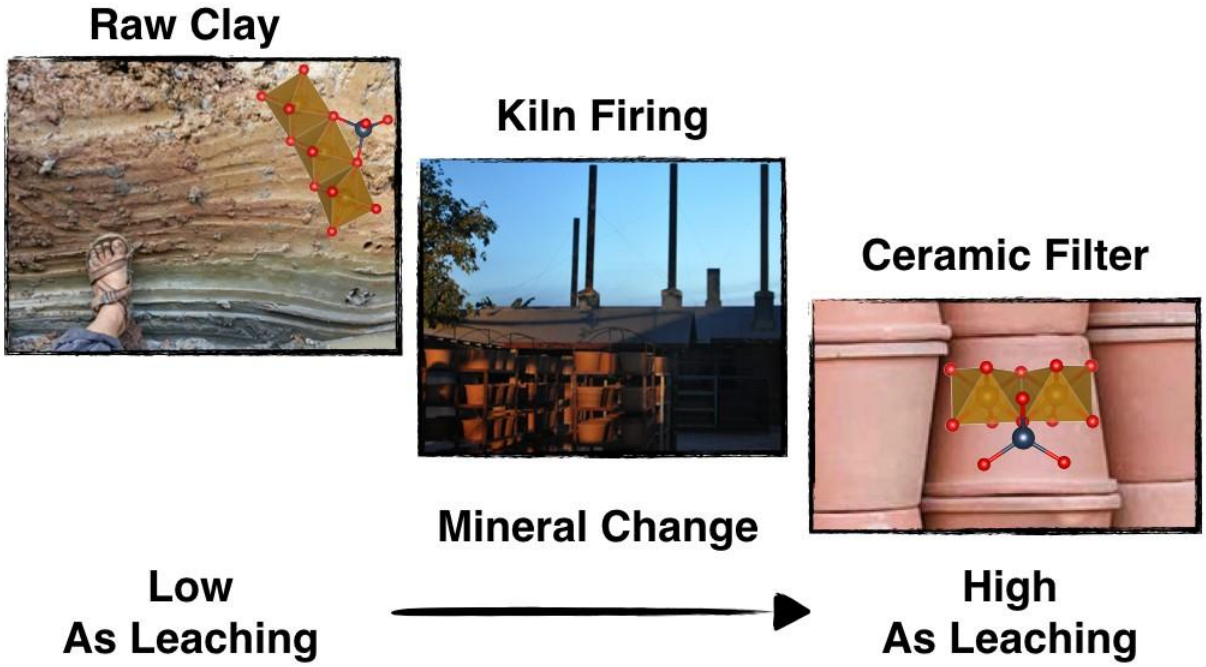

Figure 7. Schematic overview of the processes leading to increased arsenic leaching from ceramic water filters.

Fortunately, As exposure is limited to the soluble mass of As contained within a filter, and once the soluble mass is leached additional human exposure only occurs following filter replacement. In terms of limiting overall As exposure in a region with groundwater As contamination, this provides an advantage for CWFs. Whereas groundwater As can be approximated as an “infinite” source of As (i.e. the As concentration does not change significantly as a function of use or how much water is consumed), the As leached from CWFs is finite and “washes out” as more water is passed through the filter. A major component to limiting As exposure from CWFs is therefore the design life or replacement period for CWFs. The longer the interval between CWF replacement, the less As exposure from CWFs (Figure 8).

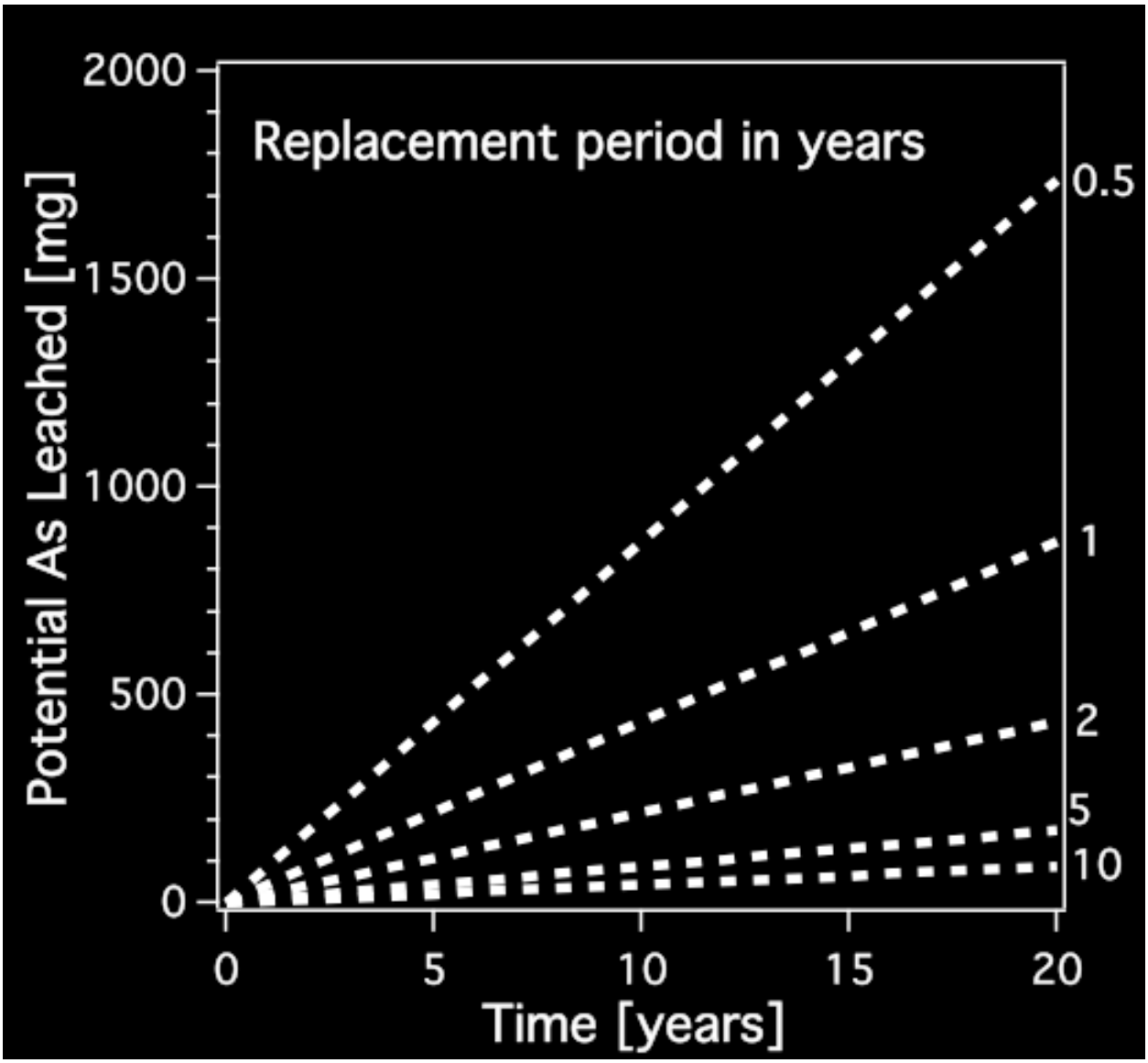

Figure 8. Relationship of total mass of arsenic leached (based on 43 mg of leachable arsenic per filter[7]) as a function of time of filter use (x-axis) for different replacement periods ranging from 6 months to 10 years.

CWFs are not used solely in regions with groundwater As contamination because the purpose of CWFs is for pathogen removal. In the case that CWFs leach As and are used in a region with no other significant As exposure pathway, the problem may be viewed differently in terms of risk analysis because CWFs introduce a potentially significant source of As rather than offsetting another existing source. Care should be taken to quantify and include the risk associated with As exposure, including estimates of total As exposure, filter replacement period, and number of household users sharing a filter to determine whether overall risk of negative outcomes associated with drinking water is improved.

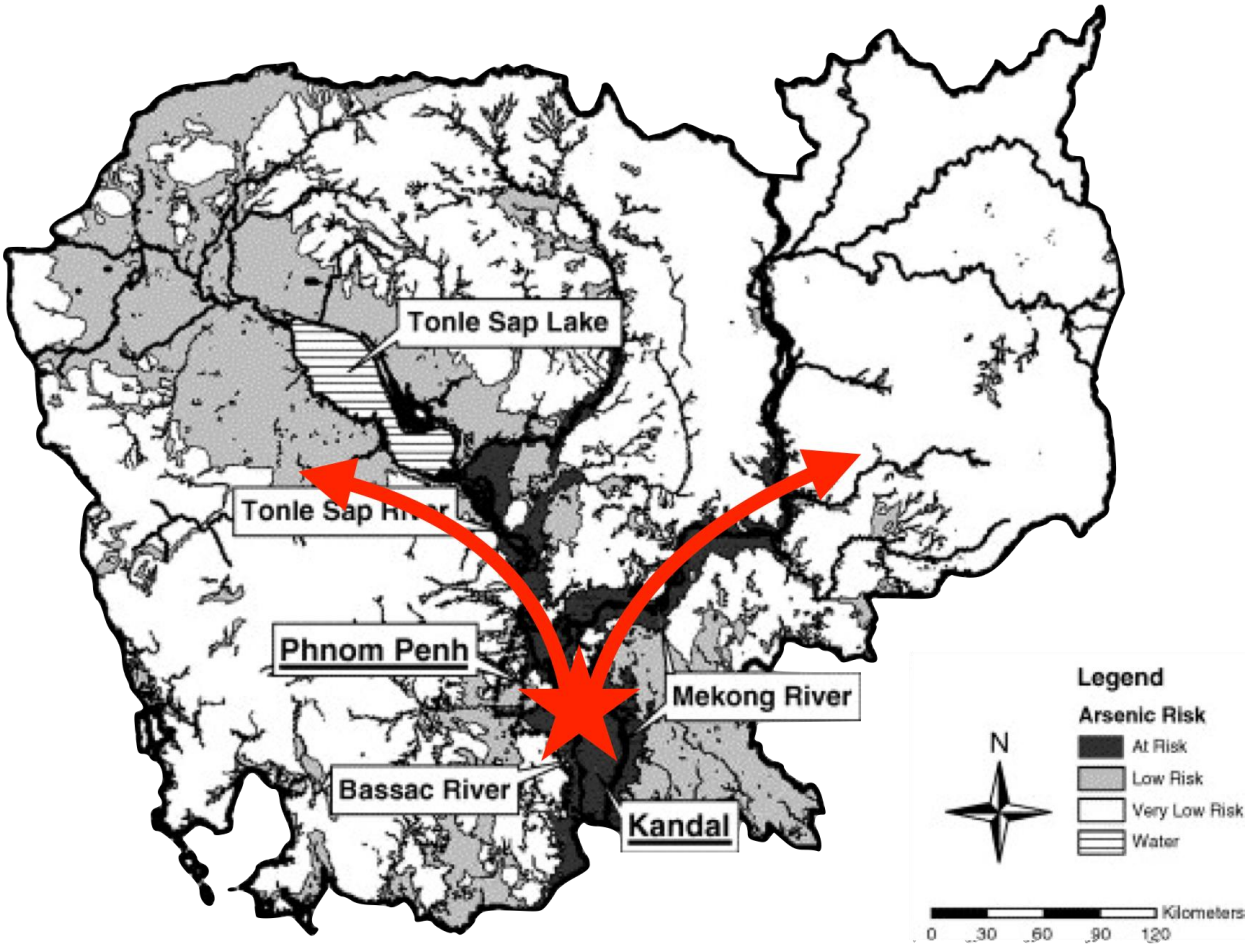

Figure 9. Example of arsenic export from CWF production facility (red star) to regions with low groundwater arsenic risk. Base map and arsenic risk data taken from Berg et al. 2007 where lighter regions have lower arsenic risk[30].

The mechanistic insight provided in this study through a combination of chemical extractions and X-ray techniques aids in (1) predicting or identifying locations where CWF production with local clay may pose a risk of As exposure and (2) providing mechanistic understanding for designing controlled leaching systems for use prior to end-user distribution. Importantly, clay solid-phase As concentrations do not need to be extraordinary to result in release of significant (i.e. hazardous) amounts of As after firing, so "low" solid-phase As concentrations in clay do not predict As leaching *a priori*. Adjustments to firing protocol (e.g. temperature) or addition of amendments to the CWF mix may provide potential mitigation strategies that should be evaluated further.

Acknowledgements

The authors thank Miranda Aiken and Abdi Garniwan for help with sample analysis and Sharon Bone, Ryan Davis, Matthew Lattimer, and Erik Nelson for help with data collection at SSRL. The authors also thank the staff at Resource Development International – Cambodia for providing samples of source clay and CWF. In particular, the authors acknowledge Marc Hall, Ann Hall, Andrew Shantz, Dina Kuy, Nuon Phen, and Som Vanna. Portions of this research were carried out at the Stanford Synchrotron Radiation Lightsource, a Directorate of SLAC National Accelerator Laboratory and an Office of Science User Facility operated for the U.S. Department of Energy Office of Science by Stanford University. M.V.S. was supported in part by the John D. Montgomery Postdoctoral Fellowship from the Pacific Basin Research Center, Soka University of America. N.L. was supported by the President's Undergraduate Research Fund, Soka University of America.

References

(1) Lye, D. J. Health Risks Associated with Consumption of Untreated Water from Household Roof Catchment Systems1. *JAWRA Journal of the American Water Resources Association* 2002, *38* (5), 1301–1306. https://doi.org/10.1111/j.1752-1688.2002.tb04349.x.

(2) Hagan, J. M.; Harley, N.; Hughes, R.; Chouhan, A.; Pointing, D.; Sampson, M. L.; Smith, K.; Saom, V. Resource Development International - Cambodia Ceramic Water Filter Handbook. Resource Development International - Cambodia 2010.

(3) Oyanedel-Craver, V. A.; Smith, J. A. Sustainable Colloidal-Silver-Impregnated Ceramic Filter for Point-of-Use Water Treatment. *Environ. Sci. Technol.* 2008, *42* (3), 927–933. https://doi.org/10.1021/es071268u.

(4) Brown, J. M. *Effectiveness of Ceramic Filtration for Drinking Water Treatment in Cambodia*; ProQuest, 2007.

(5) van Halem, D.; Heijman, S. G. J.; Soppe, A. I. A.; van Dijk, J. C.; Amy, G. L. Ceramic Silver-Impregnated Pot Filters for Household Drinking Water Treatment in Developing Countries: Material Characterization and Performance Study. *Water Science & Technology: Water Supply* 2007, *7* (5–6), 9. https://doi.org/10.2166/ws.2007.142.

(6) Archer, A. R.; Elmore, A. C.; Bell, E.; Rozycki, C. Field Investigation of Arsenic in Ceramic Pot Filter-Treated Drinking Water. *Water Science & Technology* 2011, *63* (10), 2193. https://doi.org/10.2166/wst.2011.406.

(7) Schaefer, M. V.; Shantz, A.; Fendorf, S.; Ying, S. C. Arsenic Leaching from Ceramic Water Filters. *Environ. Sci.: Water Res. Technol.* 2017. https://doi.org/10.1039/C7EW00176B.

(8) Naujokas, M. F.; Anderson, B.; Ahsan, H.; Aposhian, H. V.; Graziano, J. H.; Thompson, C.; Suk, W. A. The Broad Scope of Health Effects from Chronic Arsenic Exposure: Update on a Worldwide Public Health Problem. *Environmental Health Perspectives* 2013, *121* (3), 295–302. https://doi.org/10.1289/ehp.1205875.

(9) Tsai, S.-M.; Wang, T.-N.; Ko, Y.-C. Mortality for Certain Diseases in Areas with High Levels of Arsenic in Drinking Water. *Archives of Environmental Health: An International Journal* 1999, *54* (3), 186–193. https://doi.org/10.1080/00039899909602258.

(10) Steinmaus, C.; Ferreccio, C.; Yuan, Y.; Acevedo, J.; González, F.; Perez, L.; Cortés, S.; Balmes, J. R.; Liaw, J.; Smith, A. H. Elevated Lung Cancer in Younger Adults and Low Concentrations of Arsenic in Water. *Am. J. Epidemiol.* 2014, *180* (11), 1082–1087. https://doi.org/10.1093/aje/kwu238.

(11) Steinmaus, C.; Moore, L.; Hopenhayn-Rich, C.; Biggs, M. L.; Smith, A. H. Arsenic in Drinking Water and Bladder Cancer: Environmental Carcinogenesis. *Cancer investigation* 2000, *18* (2), 174–182.

(12) Ferreccio, C.; Smith, A. H.; Durán, V.; Barlaro, T.; Benítez, H.; Valdés, R.; Aguirre, J. J.; Moore, L. E.; Acevedo, J.; Vásquez, M. I.; Pérez, L.; Yuan, Y.; Liaw, J.; Cantor, K. P.; Steinmaus, C. Case-Control Study of Arsenic in Drinking Water and Kidney Cancer in Uniquely Exposed Northern Chile. *Am. J. Epidemiol.* 2013, kwt059. https://doi.org/10.1093/aje/kwt059.

(13) Bates, M. N.; Smith, A. H.; Hopenhaynrich, C. ARSENIC INGESTION AND INTERNAL CANCERS - A REVIEW. *American Journal of Epidemiology* 1992, *135* (5), 462–476.

(14) Navas-Acien, A.; Sharrett, A. R.; Silbergeld, E. K.; Schwartz, B. S.; Nachman, K. E.; Burke, T. A.; Guallar, E. Arsenic Exposure and Cardiovascular Disease: A Systematic Review of the Epidemiologic Evidence. *Am J Epidemiol* 2005, *162* (11), 1037–1049. https://doi.org/10.1093/aje/kwi330.

(15) Kozul, C. D.; Ely, K. H.; Enelow, R. I.; Hamilton, J. W. Low-Dose Arsenic Compromises the Immune Response to Influenza A Infection in Vivo. *Environmental Health Perspectives* 2009, *117* (9), 1441–1447.

(16) Navas-Acien A; Silbergeld EK; Pastor-Barriuso R; Guallar E. ARsenic Exposure and Prevalence of Type 2 Diabetes in Us Adults. *JAMA* 2008, *300* (7), 814–822. https://doi.org/10.1001/jama.300.7.814.

(17) Ravel, B.; Newville, M. ATHENA, ARTEMIS, HEPHAESTUS: Data Analysis for X-Ray Absorption Spectroscopy Using IFEFFIT. *Journal of synchrotron radiation* 2005, *12* (4), 537–541.

(18) Rehr, J. J.; Albers, R. C.; Zabinsky, S. I. High-Order Multiple-Scattering Calculations of x-Ray-Absorption Fine Structure. *Phys. Rev. Lett.* 1992, *69* (23), 3397–3400. https://doi.org/10.1103/PhysRevLett.69.3397.
(19) Baur, W. H.; Khan, A. A. On the Crystal Chemistry of Salt Hydrates. VI. The Crystal Structures of Disodium Hydrogen Orthoarsenate Heptahydrate and of Disodium Hydrogen Orthophosphate Heptahydrate. *Acta Cryst B* 1970, *26* (10), 1584–1596. https://doi.org/10.1107/S0567740870004521.
(20) Dainyak, L. G.; Zviagina, B. B.; Rusakov, V. S.; Drits, V. A. Interpretation of the Nontronite-Dehydroxylate Mössbauer Spectrum Using EFG Calculations. *European Journal of Mineralogy* 2006, *18* (6), 753–764. https://doi.org/10.1127/0935-1221/2006/0018-0753.
(21) Masquelier, C.; d'Yvoire, F.; Collin, G. Crystal Structure of Na7Fe4(AsO4)6 and **α**-Na3Al2(AsO4)3, Two Sodium Ion Conductors Structurally Related to II-Na3Fe2(AsO4)3. *Journal of Solid State Chemistry* 1995, *118* (1), 33–42. https://doi.org/10.1006/jssc.1995.1307.
(22) Pekov, I. V.; Zubkova, N. V.; Yapaskurt, V. O.; Belakovskiy, D. I.; Lykova, I. S.; Vigasina, M. F.; Sidorov, E. G.; Pushcharovsky, D. Y. New Arsenate Minerals from the Arsenatnaya Fumarole, Tolbachik Volcano, Kamchatka, Russia. I. Yurmarinite, Na7(Fe3+,Mg,Cu)4(AsO4)6. *Mineralogical Magazine* 2014, *78* (4), 905–917. https://doi.org/10.1180/minmag.2014.078.4.10.
(23) Jansen, E.; Kyek, A.; Schäfer, W.; Schwertmann, U. The Structure of Six-Line Ferrihydrite. *Appl Phys A* 2002, *74* (1), s1004–s1006. https://doi.org/10.1007/s003390101175.
(24) Wechsler, B. A.; Lindsley, D. H.; Prewitt, C. T. Crystal Structure and Cation Distribution in Titanomagnetites (Fe3-XTixO4). *American Mineralogist* 1984, *69* (7–8), 754–770.
(25) Maslen, E. N.; Streltsov, V. A.; Streltsova, N. R.; Ishizawa, N. Synchrotron X-Ray Study of the Electron Density in **α**-Fe2O3. *Acta Cryst B* 1994, *50* (4), 435–441. https://doi.org/10.1107/S0108768194002284.
(26) Baccour, H.; Medhioub, M.; Jamoussi, F.; Mhiri, T. Influence of Firing Temperature on the Ceramic Properties of Triassic Clays from Tunisia. *Journal of Materials Processing Technology* 2009, *209* (6), 2812–2817. https://doi.org/10.1016/j.jmatprotec.2008.06.055.
(27) Wattanasiriwech, D.; Srijan, K.; Wattanasiriwech, S. Vitrification of Illitic Clay from Malaysia. *Applied Clay Science* 2009, *43* (1), 57–62. https://doi.org/10.1016/j.clay.2008.07.018.
(28) Pinakidou, F.; Katsikini, M.; Paloura, E. C.; Kalogirou, O.; Erko, A. On the Local Coordination of Fe in Fe2O3-Glass and Fe2O3-Glass Ceramic Systems

Containing Pb, Na and Si. *Journal of Non-Crystalline Solids* 2007, *353* (28), 2717–2733. https://doi.org/10.1016/j.jnoncrysol.2007.05.007.

(29) Pekov, I. V.; Koshlyakova, N. N.; Zubkova, N. V.; Lykova, I. S.; Britvin, S. N.; Yapaskurt, V. O.; Agakhanov, A. A.; Shchipalkina, N. V.; Turchkova, A. G.; Sidorov, E. G. Fumarolic Arsenates − a Special Type of Arsenic Mineralization. *European Journal of Mineralogy* 2018, *30* (2), 305–322. https://doi.org/10.1127/ejm/2018/0030-2718.

(30) Berg, M.; Stengel, C.; Trang, P. T. K.; Viet, P. H.; Sampson, M. L.; Leng, M.; Samreth, S.; Fredericks, D. Magnitude of Arsenic Pollution in the Mekong and Red River Deltas—Cambodia and Vietnam. *Science of the Total Environment* 2007, *372* (2), 413–425.